Table 4-1. Migration types.

Type	Discussion
Stack	The section the interpreter always wants.
Depth Conversion Along Vertical Raypaths	Strictly valid only for velocity that varies with depth, without structural dip.
Time Migration	Needed when the stacked section contains diffractions or structural dip. Valid for vertically varying velocity. Acceptable for mild lateral velocity variations.
Depth Migration	Needed when the stacked section contains structural dip and large lateral velocity gradients.
Prestack Partial Migration (PSPM)	Poststack migration is acceptable when the stacked section is equivalent to a zero-offset section. This is not the case for conflicting dips with different stacking velocities or large lateral velocity gradients. PSPM [Dip Moveout (DMO)] provides a better stack that can be migrated after stack. However, PSPM only solves the problem of conflicting dips with different stacking velocities.
Full-Time Migration Before Stack	The output is a migrated section. No intermediate unmigrated stacked section is produced. This often is not what the interpreter wants; he must have an unmigrated stacked section and its migrated form. Nevertheless, this is the rigorous solution to the problem of conflicting dips. PSPM is a simplification of this process.
Depth Migration Before Stack	Needed when there are extremely strong lateral velocity gradients that cannot be treated properly by stacking.
3-D Time Migration After Stack	Needed when the stack contains dipping events that are out of the profile plane (crossdips). After stack, this is the most common type of 3-D migration.
3-D Depth Migration After Stack	Needed when the problem of strong lateral velocity variation involves 3-D subsurface structural complexity.
3-D Time Migration Before Stack	Needed when PSPM fails and when the stack contains crossdips.
3-D Depth Migration Before Stack	What everyone would like to have if computer time were abundant and if the 3-D subsurface velocity model were known accurately.

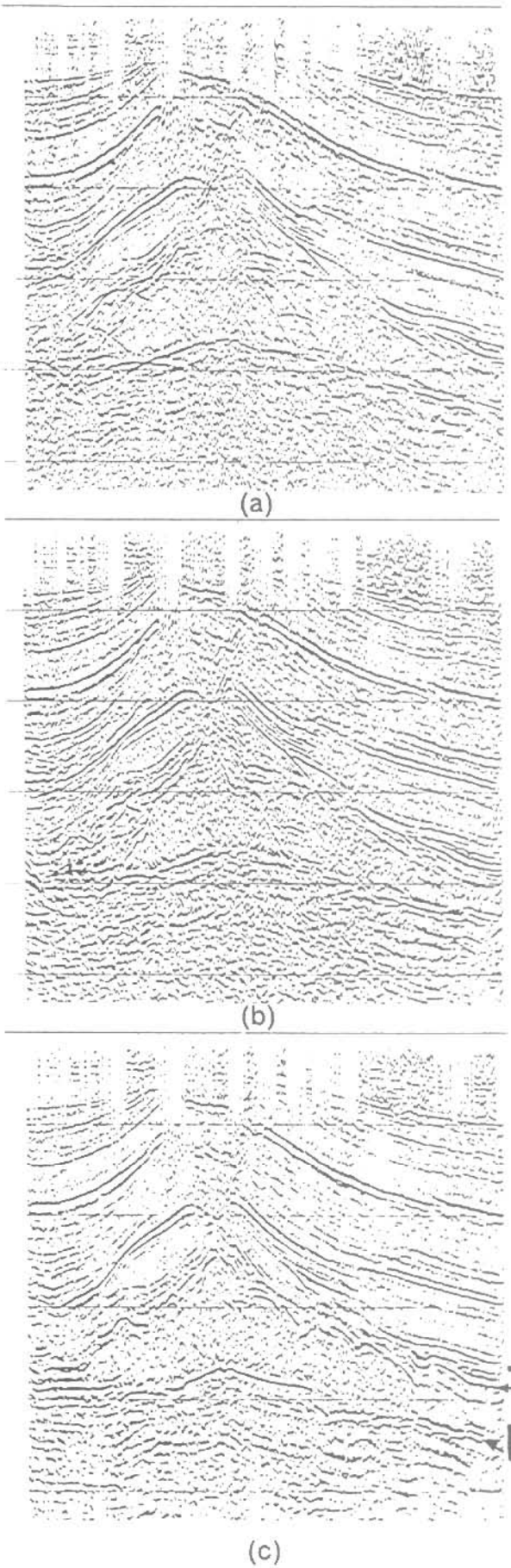

FIG. 4-6. A 2-D CMP stack (a) truly represents a 3-D wave field cross section. Thus, it can contain energy from outside the 2-D profile plane. A 2-D migration (b) is inadequate when this kind of energy is present on the 2-D CMP stacked section. (c) Clear imaging of the salt structure requires both 3-D data collection and 3-D migration (Chapter 6). (Data courtesy Nederlandse Aardolie Maatschappij B.V.)

to the depth axis is done by using the relation $z = v\tau/2$. We will examine the horizontal and vertical displacements as seen on the migrated time section. The amount of horizontal and vertical displacement that takes place in migrating dipping reflector $C'D'$ to its true subsurface position CD can be quantified. From Figure 4-15, consider a reflector segment AB. Assume that AB migrates to $A'B'$ and that point C on AB migrates to point C' on $A'B'$. The horizontal and vertical (time) displacements d_x and d_t and the dip angle after migration $\bar{\theta}_t$ (all measured on the migrated time section) can be expressed in terms of medium velocity v, traveltime t, and apparent dip of the reflector as seen on the unmigrated time section θ_t. Chun and Jacewitz (1981) derived the following formulas:

$$d_x = (v^2 t \tan \theta_t)/4 \tag{4.1}$$

$$d_t = t\{1 - [1 - (v^2 \tan^2 \theta_t)/4]^{1/2}\} \tag{4.2}$$

$$\tan \bar{\theta}_t = \tan \theta_t / [1 - (v^2 \tan^2 \theta_t)/4]^{1/2}, \tag{4.3}$$

where $\tan \theta_t = \Delta t/\Delta x$, as measured on the unmigrated time section.

To gain a better understanding of these expressions, we consider a numerical example. For a realistic velocity function that increases with depth, consider five reflecting segments at various depths. For simplicity, assume that quantity $\Delta t/\Delta x$ is the same for all (10 ms per 25-m trace spacing). From the expressions in equations (4.1), (4.2), and (4.3), compute the horizontal and vertical displacements d_x and d_t and the dips (in ms/trace) after migration. The results are summarized in Table 4-2.

Table 4-2. Horizontal and vertical displacements of points on dipping reflectors at various depths and changes in dip angle as measured on a time section as a result of migration.

t (s)	v (m/s)	d_x (m)	d_t (s)	θ_t (ms/trace)	$\bar{\theta}_t$ (ms/trace)
1	2500	625	0.134	10	11.5
2	3000	1800	0.400	10	12.5
3	3500	3675	0.858	10	14.0
4	4000	6400	1.600	10	16.7
5	4500	10125	2.820	10	23.0

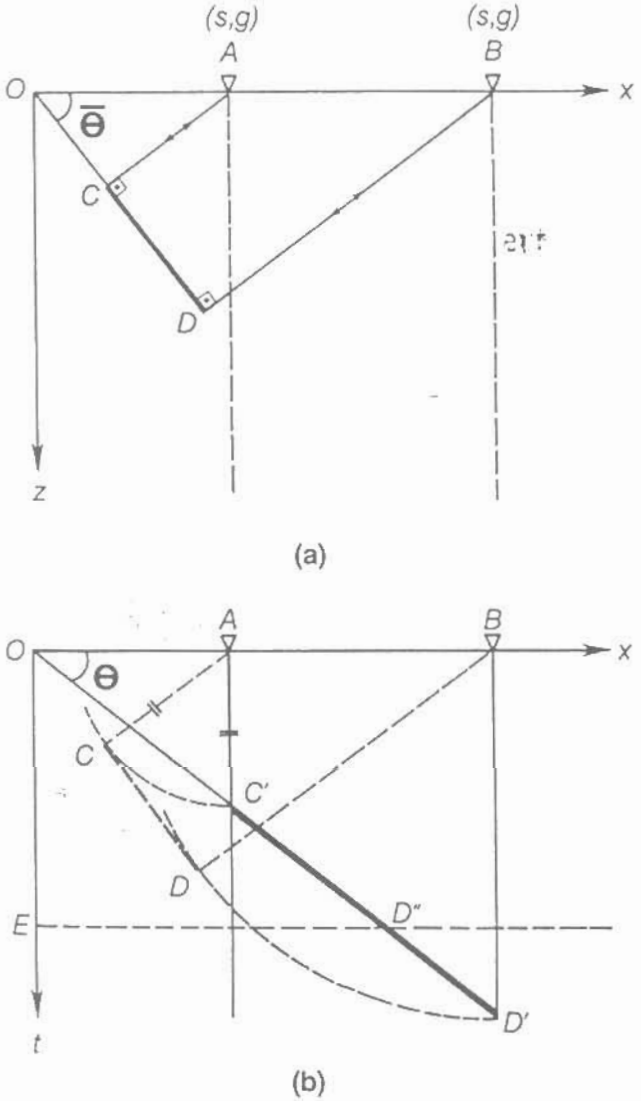

FIG. 4-14. Migration principles: The reflection segment $C'D'$ in the time section (b), when migrated, is moved updip, steepened, shortened, and mapped onto its true subsurface location CD (a). (Adapted from Chun and Jacewitz, 1981.)

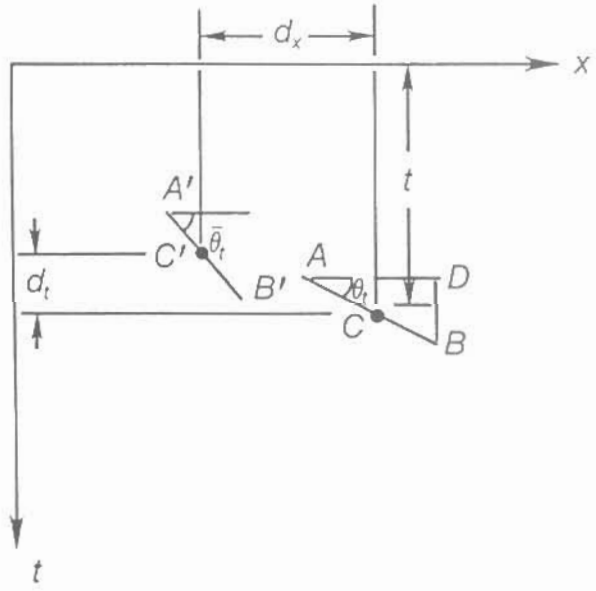

FIG. 4-15. Quantitative analysis of the migration process. Point C on dipping reflector AB is moved to C' after migration. The amount of horizontal displacement d_x, vertical displacement d_t, and dip angle after migration $\bar{\theta}_t$ is calculated from equations (4.1), 4.2), and (4.3). Here, $\Delta x = AD$, $\Delta t = BD$.

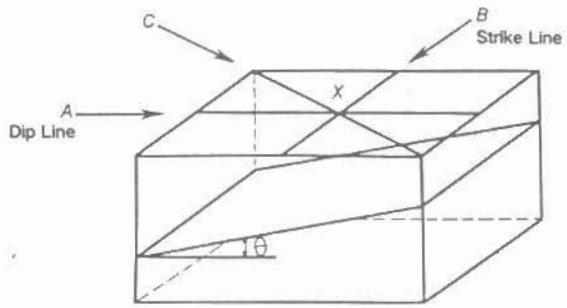

FIG. 6-1. A subsurface model consisting of a single dipping plane interface in a homogeneous medium. Line A is in the dip direction, line B is in the strike direction, and line C is in an arbitrary direction. After migration, data recorded at the intersection point X on these three lines migrate to positions corresponding to different subsurface locations. Schematic illustrations of the migrations are shown in Figures 6-2 and 6-3. (Adapted from Workman, 1984.)

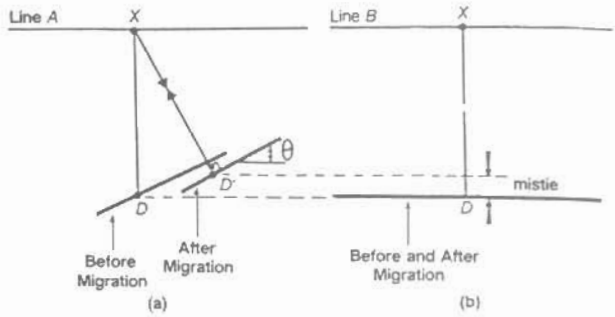

FIG. 6-2. (a) Migration along the dip line and (b) along the strike line over the depth model in Figure 6-1. Point D after migration is moved updip to D′ along dip line A. Point D does not move after migration along strike line B. This causes the mistie indicated between the two migrated sections.

Although principles of 3-D migration are discussed in Section 6.5, we need to assess the interpretational differences between 2-D and 3-D migrations. Figure 6-4 shows an in-line (left column) and a cross-line (right column) stacked section from a land 3-D survey and their 2-D and 3-D migrations. Note that 3-D migration has yielded a better definition of the top (T) of the salt dome and better delineation of the faults along the base (B) of the salt dome. There is no doubt that the interpretation based on 2-D imaging is significantly different from interpretation based on 3-D imaging.

Figure 6-5 is another example of the significant improvement available from the interpretation of a 3-D migrated section. Note that the two salt domes and the syncline between are delineated better after 3-D migration. Three-dimensional migration often produces surprisingly different sections from 2-D migrated sections. The example in Figure 6-6 shows a no-reflection zone on the 2-D migrated section, while the same zone contains a series of continuous reflections on the 3-D migrated section that are easily correlated with reflections outside that zone.

As noted earlier, 2-D migration can introduce misties between 2-D lines in the presence of dipping events. Two-dimensional migration cannot adequately image the subsurface, while 3-D migration eliminates these misties by completing the imaging process. This is demonstrated in Figure 6-7 in which the correlation of an in line and a cross line can be examined at their intersection (indicated by the vertical bar). The slight mistie problem that is evident on the 2-D migrated sections (especially apparent between 1.3 and 2 s) is eliminated on the 3-D migrated sections.

From the field data examples, we see that 3-D migration provides complete imaging of the 3-D subsurface geology. In contrast, 2-D migration can yield inadequate results. The difference between 2-D seismic and 3-D seismic is the way in which migration is performed.

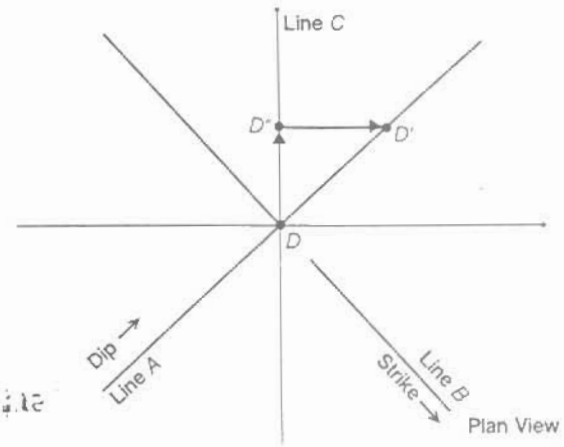

FIG. 6-3. Plan view of the migrations at the intersection point along the three lines indicated in Figure 6-1. Point D moves to D′, its true subsurface position, along dip line A. Point D does not move on strike line B. The same point moves to D″ along line C, which is in an arbitrary direction. Complete imaging is achieved by migrating the data again along the direction perpendicular to C to move the energy from D″ to D′.

Dense coverage on top of the target zone, say a 25-m in-line trace spacing and a 25-m cross-line trace spacing, will not necessarily provide adequate subsurface imaging unless migration is performed in a 3-D sense.

Figure 6-8 shows an increasingly modified and improved interpretation made from seismic data that were obtained from detailed 2-D surveys in an area between 1964 and 1970. The reconnaissance survey in the first year of exploration (1964) consisted of only a few lines. A preliminary time structure map based on this initial survey inferred a structural closure with a northwesterly trend. In the second year of exploration (1965), more lines were shot in the same directions as before and the structural closure was verified somewhat. Lines were

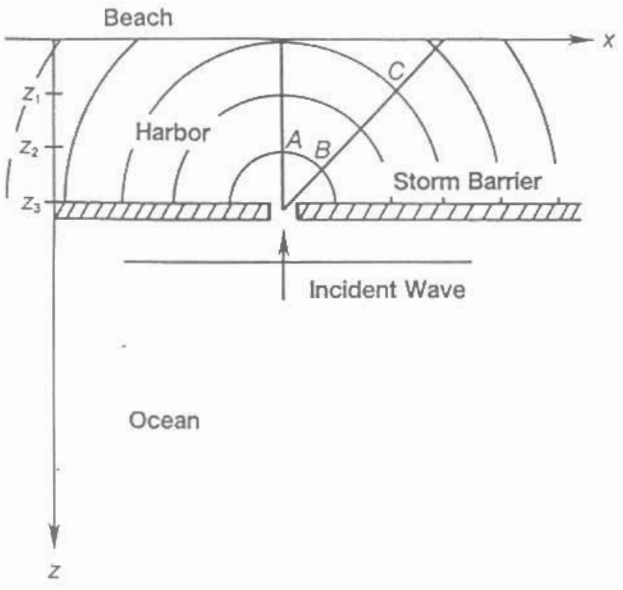

FIG. 4.1-9. The gap in the barrier acts as Huygens' secondary source, causing the circular wavefronts that approach the beach line. (Adapted from Claerbout, 1985.)

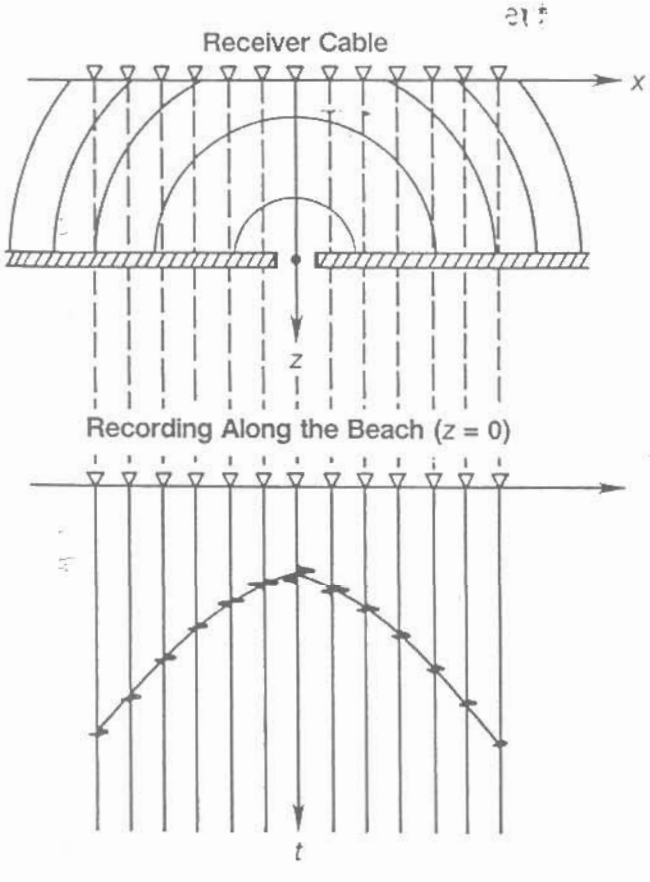

FIG. 4.1-10. Waves recorded along the beach generated by Huygens' secondary source (the gap in the barrier in Figure 4.1-9) have a hyperbolic traveltime trajectory.

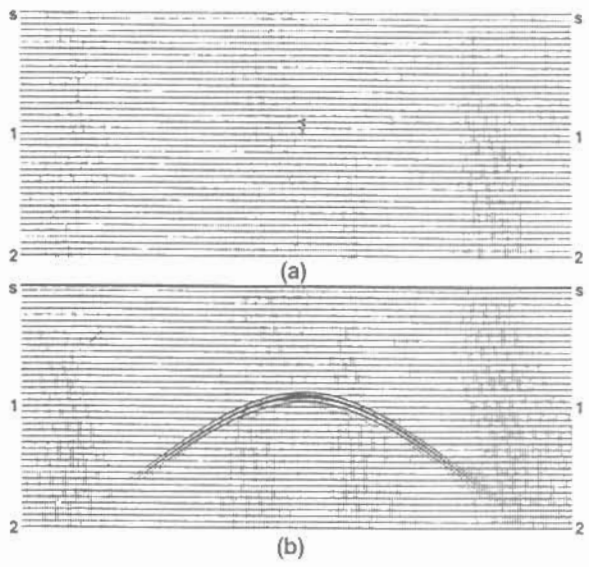

FIG. 4.1-11. A point that represents a Huygens' secondary source (a) produces a diffraction hyperbola on the zero-offset time section (b). The vertical axis in this section is two-way time, while the vertical axis in the time section in Figure 4.1-10 is one-way time.

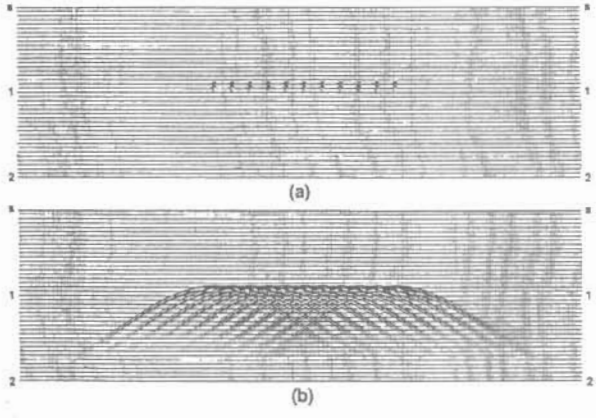

FIG. 4.1-12. Superposition of the zero-offset responses (b) of a discrete number of Huygens' secondary sources as in (a).

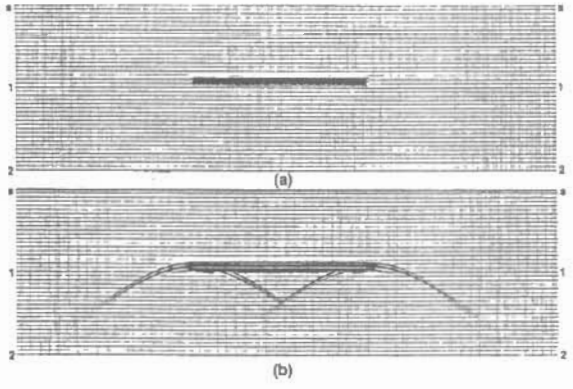

FIG. 4.1-13. Superposition of the zero-offset responses (b) of a continuum of Huygens' secondary sources as in (a).

Diffraction Summation

Huygens' secondary source signature is a semicircle in the $x - z$ plane and a hyperbola in the $x - t$ plane. This characterization of point sources in the subsurface leads to two practical migration schemes. Figure 4.1-14a shows a zero-offset section that consists of a single arrival at a single trace. This event migrates to a semicircle (Figure 4.1-14b). From Figure 4.1-14, note that the zero-offset section recorded over a constant-velocity earth model consisting of a semicircular reflecting interface contains a single blip of energy at a single trace as in Figure 4.1-14a. Since this recorded section consists of an impulse, the migrated section in Figure 4.1-14b can be called the *migration impulse response*. An alternate scheme for migration results from the observation that a zero-offset section consisting of a single diffraction hyperbola migrates to a single point (Figure 4.1-15b).

The first method of migration is based on the superposition of semicircles, while the second method is based on the summation of amplitudes along hyperbolic paths. The first method was used before the age of digital computers. The second method, which is known as the *diffraction summation method*, was the first computer implementation of migration.

The migration scheme based on the semicircle superposition consists of mapping the amplitude at a sample in the input $x - t$ plane of the unmigrated time section onto a semicircle in the output $x - z$ plane. The migrated section is formed as a result of the superposition of the many semicircles.

The migration scheme based on diffraction summation consists of searching the input data in the $x - t$ plane for energy that would have resulted if a diffracting source (Huygens' secondary source) were located at a particular point in the output $x - z$ plane. This search is carried out by summing the amplitudes in the $x - t$ plane along the diffraction curve that corresponds to Huygens' secondary source at each point in the $x - z$ plane. The result of this summation then is mapped onto the corresponding point in the $x - z$ plane. As noted early in this section, within the context of time migration, however, the summation result actually is mapped onto the $x - \tau$ plane, where τ is the event time in the migrated position.

The curvature of the hyperbolic trajectory for amplitude summation is governed by the velocity function. The equation for this trajectory can be derived from the geometry of Figure 4.1-15. A formal derivation also is provided in Section D.2. Assuming a horizontally layered velocity-depth model, the velocity function used to compute the traveltime trajectory is the rms velocity at the apex of the hyperbola at time τ (Section 3.1).

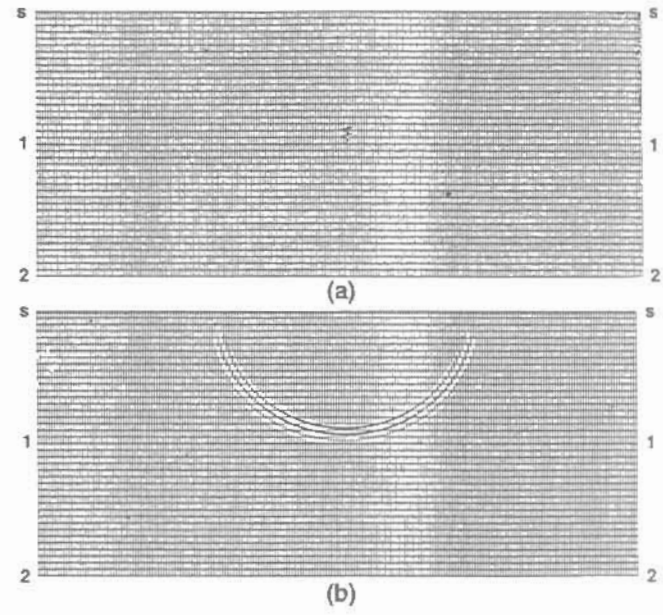

FIG. 4.1-14. Principles of migration based on semicircle superposition. (a) Zero-offset section (trace interval, 25 m; constant velocity, 2500 m/s), (b) migration.

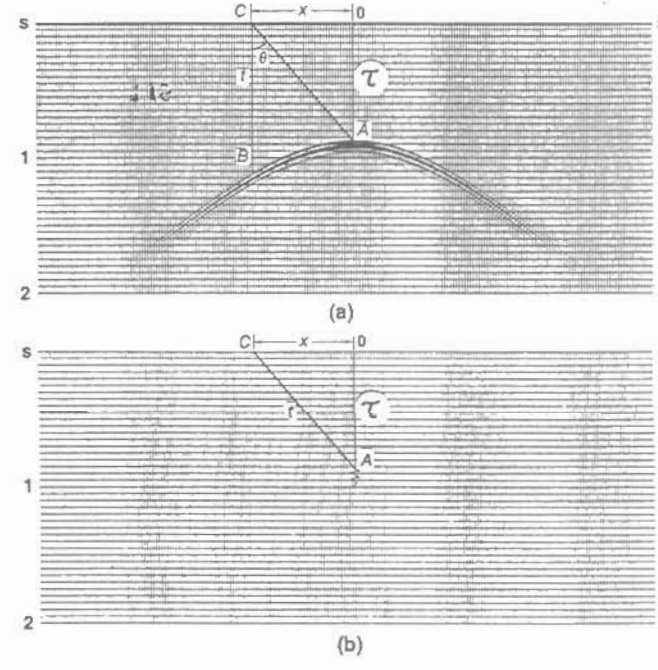

FIG. 4.1-15. Principles of migration based on diffraction summation. (a) Zero-offset section (trace interval, 25 m; constant velocity, 2500 m/s). (b) migration. The amplitude at input trace location B along the flank of the traveltime hyperbola is mapped onto output trace location A at the apex of the hyperbola by equation (4-4).

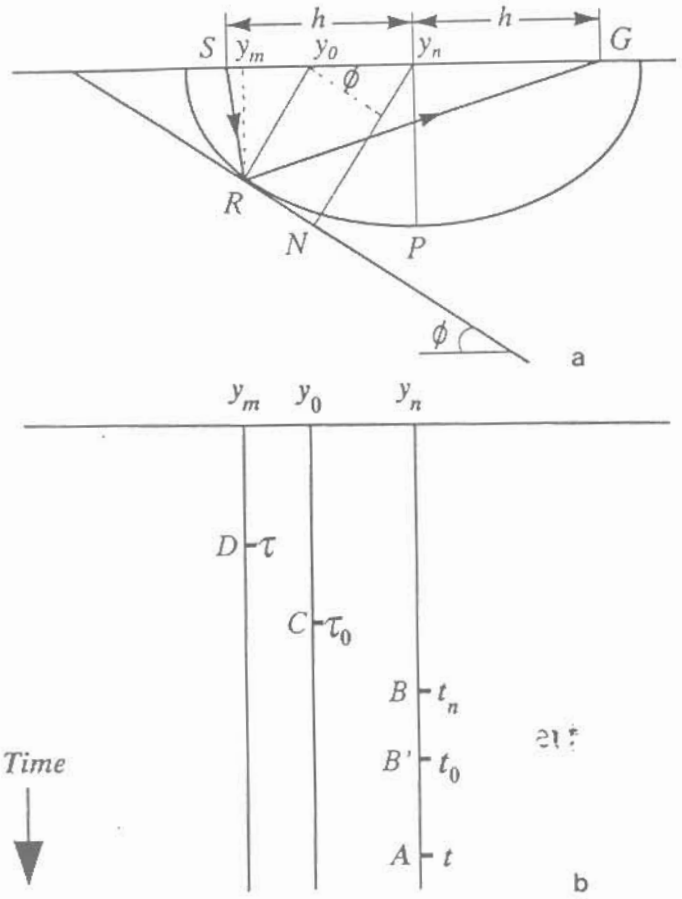

FIG. 5.1-1. (a) The geometry of a nonzero-offset recording of reflections from a dipping layer boundary; (b) a sketch of the time section depicting the various traveltimes. NMO correction involves coordinate transformation from $y_n - t$ to $y_n - t_n$ by mapping amplitude A at time t to B at time t_n on the same trace. DMO correction involves coordinate transformation from $y_n - t_n$ to $y_0 - \tau_0$ by mapping amplitude B at time t_n on the trace at midpoint location y_n of the moveout-corrected common-offset section to amplitude C at time τ_0 on the trace at midpoint location y_0 of the zero-offset section. Zero-offset migration involves coordinate transformation from $y_0 - \tau_0$ to $y_m - \tau$ by mapping amplitude C at time τ_0 on the trace at midpoint location y_0 of the zero-offset section to amplitude D at time τ on the trace at midpoint location y_m of the migrated section. Migration before stack involves direct mapping of amplitude A at time t on the trace at midpoint location y_n of the common-offset section to amplitude D at time τ on the trace at midpoint location y_m of the migrated section. See text for the relationships between the coordinate variables.

(b) *Dip-moveout correction* that maps the amplitude at time t_n denoted by the sample B on the trace at midpoint y_n of the moveout-corrected common-offset section with offset $2h$ to time τ_0 denoted by the sample C on the trace at midpoint y_0 of the zero-offset section.

Zero-offset migration then maps the amplitude at time τ_0 denoted by the sample C on the trace at midpoint y_0 of the zero-offset section to the amplitude at time τ denoted by the sample D on the trace at midpoint y_m of the migrated section. Note that the combination of NMO correction. DMO correction, and zero-offset migration achieves the same objective as direct mapping of the amplitude at time t denoted by the sample A on the trace at midpoint y_n of the common-offset section with offset $2h$ to the amplitude at time τ denoted by the sample D on the trace at midpoint y_m of the migrated section. This direct mapping procedure is the basis of algorithms for migration before stack (Section 5.3).

The important point to note is that the normal-moveout correction in step (a) is performed using the velocity of the medium above the dipping reflector.

The NMO equation (3-8) defines the traveltime t from source location S to the reflection point R to the receiver location G. This equation, written in prestack data coordinates, is

$$t^2 = t_0^2 + \frac{4h^2 \cos^2 \phi}{v^2}, \qquad (5-1)$$

where $2h$ is the offset, v is the medium velocity above the reflector, ϕ is the reflector dip, and t_0 is the two-way zero-offset time at midpoint location y_n.

Dip-moveout correction of step (b) is preceded by zero-dip normal-moveout correction of step (a) using the dip-independent velocity v:

$$t^2 = t_n^2 + \frac{4h^2}{v^2}, \qquad (5-2)$$

where t_n is the event time at midpoint y_n after the NMO correction. Event time t_n after the NMO correction and event time t_0 are related as follows (Section E.2)

$$t_n^2 = t_0^2 - \frac{4h^2 \sin^2 \phi}{v^2}. \qquad (5-3)$$

At first glance, equations (5-2) and (5-3) suggest a two-step approach to moveout correction:

(a) Apply a *dip-independent* moveout correction using equation (5-2) to map the amplitude at time t denoted by the sample A on the trace at midpoint y_n of the common-offset section with offset $2h$ to time t_n denoted by the sample B on the same trace at midpoint y_n of the same common-offset section.
(b) Apply a *dip-dependent* moveout correction using equation (5-3) to map the amplitude at time t_n denoted by the sample B on the trace at midpoint y_n of the moveout-corrected common-offset section with offset $2h$ to time t_0 denoted by the sample

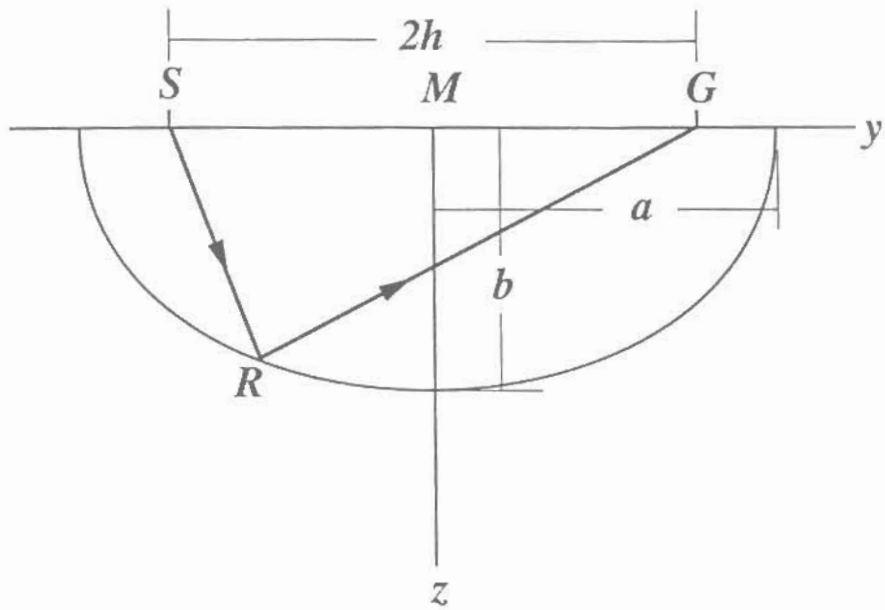

FIG. E-2. The prestack time migration ellipse. See Section E.5 for details.

Square both sides of equation (E-67) to get

$$v^2t^2 = 2\sqrt{\left[(y+h)^2+z^2\right]\left[(y-h)^2+z^2\right]} + \left[(y+h)^2+z^2\right] + \left[(y-h)^2+z^2\right]. \qquad (E-68)$$

Combine the second and third terms on the right-hand side and simplify the terms inside the square root

$$v^2t^2 = 2\sqrt{(y^2-h^2)^2 + 2z^2(y^2+h^2)+z^4} + 2(y^2+h^2+z^2). \qquad (E-69a)$$

Perform further algebraic manipulation to collect the terms in y and z

$$(v^2t^2-4h^2)y^2 + v^2t^2z^2 = \frac{v^4t^4}{4} - v^2t^2h^2. \qquad (E-69b)$$

Finally, normalize by the terms on the right-hand side and rearrange the terms in the denominators

$$\frac{y^2}{(vt/2)^2} + \frac{z^2}{(vt/2)^2-h^2} = 1. \qquad (E-70)$$

Equation (E-70) represents an ellipse in the $y-z$ plane for a constant t with the following parameters (Figure E-2):

(a) Semi-major axis in midpoint y direction: $a = vt/2$.
(b) Semi-minor axis in depth z direction: $b = \sqrt{(vt/2)^2-h^2}$.
(c) Distance from center to either focus: $\sqrt{a^2-b^2} = h$.
(d) Distance from one focus to a point on the ellipse to the other focus: vt.

The ellipse of equation (E-70) in the $y-z$ plane describes the *impulse response* of a nonzero-offset migration operator applied to prestack data.

When equation (E-70) is specialized to the zero-offset case, $h = 0$, we get

$$\frac{y^2}{(vt/2)^2} + \frac{z^2}{(vt/2)^2} = 1, \qquad (E-71a)$$